Frontiers of Physics
https://doi.org/10.1007/s11467-020-0958-4
Front. Phys.
15(2), 23604 (2020)

RESEARCH ARTICLE

$ZnGeP_2$: A near-infrared-activated photocatalyst for hydrogen production

Xin Li[1,2], Peng Wang[1,*], Ya-Qiang Wu[1], Zhen-Hua Liu[1], Qian-Qian Zhang[1], Ting-Ting Zhang[3], Ze-Yan Wang[1], Yuan-Yuan Liu[1], Zhao-Ke Zheng[1], Bai-Biao Huang[1]

[1] *State Key Laboratory of Crystal Materials, Shandong University, Jinan 250100, China*
[2] *Engineering Technology Research Center of Henan Province for Solar Catalysis, College of Chemistry and Pharmaceutical Engineering, Nanyang Normal University, Nanyang 473061, China*
[3] *Comprehensive Technical Service Center, Linyi Customs, Linyi 276034, China*
*Corresponding author. E-mail: *pengwangicm@sdu.edu.cn*
Received December 27, 2019; accepted January 19, 2020

In this work, we prepared $ZnGeP_2$ (ZGP) photocatalyst using single flat temperature zone (SFT) method in a vacuum quartz ampoule. The XRD, SEM, EDS, DRS and XPS were used to characterize the crystal structure, morphology, elemental content, optical absorption and band gap structure of ZGP. The results of photocatalytic hydrogen evolution and apparent quantum efficiency show that ZGP is a promising photocatalyst for hydrogen production both under visible and near-infrared light irradiation. In addition, it is also found that adding the common stabilizer H_3PO_2 and ultrasonic treatment can efficiently improve the photocatalytic activity and stability of ZGP.

Keywords $ZnGeP_2$, near-infrared-activated photocatalyst, H_2 production

1 Introduction

Since hydrogen production from water photolysis has been discovered on semiconductor electrode in 1972[1], photocatalytic water splitting has gained enormous attention at the aspect of directly converting solar energy resources into chemical energy. A large number of researchers, including chemist, physicist, materials scientists, and so on, have devoted themselves to exploring efficient photocatalysts for hydrogen production [2–5]. Until now, thousands of photocatalysts have been developed, such as TiO_2 [6, 7], CdS [8–10], Ag@AgCl [11], g-C_3N_4 [12, 13], $CH_3NH_2PbI_3$ [14], and $CsPbBr_{3-x}I_x$ [15]. However, the hydrogen production efficiency of most photocatalysts is not ideal. One of the important factors is the narrow scope of light absorption. The solar spectrum contains about 3%–5% ultraviolet (UV, <400 nm), 42%–43% visiblelight (Vis, 400–800 nm) and 52%–55% near infrared light (NIR, >800 nm). However, a majority of photocatalysts only absorb UV or visible light, while the near infrared light, which accounts for nearly half of the solar spectrum, is wasted. Therefore, maximize the use of sunlight is expected to be a promising strategy to improve the activity of photocatalysts, in other words, developing near-infrared-activated photocatalysts is urgent and important.

Actually, tremendous efforts have been made and numerous near-infrared-activated photocatalysts have been found. The main strategies contain introducing defect bands and vacancies [16–20], sensitization with NIR responsive organic dyes [21], constructing upconversion (UC)@semiconductor compounds [22–26] and development of photocatalysts with intrinsic infrared light absorption [27–29].

Zinc germanium phosphide, $ZnGeP_2$ (ZGP), a chalcopyrite ternary ABC_2 type compound, is among the most promising infrared nonlinear optical materials in the middleinfrared range. ZGP single crystal possesses peculiar optical quality, stable physicochemical property and excellent mechanical character [30–32], which make it widely used as an ideal non-infrared optical medium material for optical parametric oscillations, optical parameter amplification, secondary harmonic generation (SHG), and so on [33–35]. These excellent properties of ZGP inspire us to study on its photocatalytic activity of hydrogen production. Furthermore, there are hardly any reports on the application of ZGP in photocatalysis. In this paper, ZGP photocatalyst was synthesized by single flat temperature zone (SFT) method. The crystal structure, morphology, optical absorption and valence band spectrum of ZGP were also characterized. The photocatalytic activities for hydrogen production of ZGP were measured under visible and near infrared light irradiation. In addition, in order to solve the problem that ZGP is easily oxidized by photoinduced holes due to the existence of P^{3-}, we selected to add the common stabilizer H_3PO_2 into the photocatalytic reaction solution to improve its reaction stability. In addition, it was also discovered that ultrasonic treatment can effectively enhance the photocatalytic activity and stability of ZGP. Our work demonstrates ZGP could be a promising photocatalyst for applications in energy under visible and near infrared light irradiation.

2 Experimental section

Highly pure P, Zn and Ge (99.99%) were purchased from Alfa Aesar Co., Inc. N-Methyl pyrrolidone (NMP), methanol, H_2PtCl_6 and H_3PO_2 were purchased from Sinopharm Chemical Reagent Co., Ltd. All chemical materials were used without further purification unless particularly pointed out.

2.1 Preparation of bulk $ZnGeP_2$

Highly pure P, Zn and Ge (Alfa Aesar, 99.99%) were directly mixed according to stoichiometric amounts in quartz ampoule. The quartz ampoule was evacuated to a pressure lower than 2.0×10^{-2} Pa and then placed in a muffle furnace. The detailed temperature control process was as follows: initially, the temperature was raised up to 530 °C in 10 h and held for 12 h. Subsequently, the temperature was raised up to 630 °C at a rate of 4 °C/h and then to 1070 °C at a rate of 20 °C/h. Finally, after kept at 1070 °C for 8 h, the temperature was cooled to room temperature in 3 h. The product was denoted as bulk ZGP.

2.2 Preparation of ZGP powders

Firstly, the above bulk ZGP was grinded in ethanol solution thoroughly, after the ethanol evaporated, ZGP was dispersed in ethanol solution again and repeated the above process three times. After that, 20 mg of the as-prepared ZGP was dispersed in 20 mL of NMP under ultrasonic treatment for 10 h. To remove the bulk ZGP, the dispersion was centrifuged at 2000 rpm for 20 min. The supernatant sample was removed and retained carefully, and then was redispersed in NMP solution under ultrasonic treatment for 6 h. Finally, the above dispersion was centrifuged at 12 000 rpm for 20 min three times. After dried in an oven at 60 °C overnight, the ZGP powder was obtained. For the sake of distinction, the samples before and after ultrasonic treatment were labeled as ZGP (before) and ZGP (after).

2.3 Characterization of catalysts

The powder X-ray diffraction (XRD) pattern was characterized by using a Bruker AXS D8 Advance powder diffractometer with a Cu Kα X-ray tube (λ=0.154056 nm) and a step size of 0.02° at room temperature. Field emission scanning electron microscopy (FE-SEM, Hitachi, S-4800) was used to study the morphologies of as-prepared samples. UV-vis diffuse reflectance spectra (DRS) were carried out using ShimadzuUV 2600 spectrophotometer equipped with an integrating sphere, using 100% $BaSO_4$ as reflectance standard. X-ray photoelectron spectroscopy (XPS) spectra were measured in a Thermo Fisher Scientific Escalab 250 X-ray photoelectron spectrometer with a monochromatic Al Kα radiation, and C 1 s (284.6 eV) was used to calibrate the peak position of the elements.

2.4 Hydrogen evolution measurements

To evaluate the photocatalytic hydrogen evolution of ZGP samples, a reaction vessel (10 mL) sealed tightly with a rubber septum was used. In a typical photocatalytic measurement, the as-prepared sample was suspended in aqueous solution (3 mg/mL) containing 2 mL methanol as a sacrificial agent and H_2PtCl_6 (Pt 1.0 wt%) as a co-catalyst. In order to avoid the occurrence of photocorrosion, 1 mL H_3PO_2 was also added. Before the experiment began, the mixture was degassed with high purity N_2 for 30 min. The temperature was maintained at 15 °C. A 300 W Xe arc lamp (PLS-SXE 300, Beijing Trusttech Co. Ltd.) with an optical filter ($\lambda > 420$ nm or $\lambda > 800$ nm) was used to provide the visible light or near infrared light source. The amount of H_2 produced in this photocatalytic process was determined by a gas chromatograph equipped with thermal conductivity detector.

The apparent quantum efficiency (QE) was also measured under the same photocatalytic reaction conditions. A 300 W Xe arc lamp with a band-pass filter of 420 nm, 450 nm, 520 nm, 600 nm or 850 nm and a masked area of π cm^2 was used to provide irradiation light. The photon flux of the incident light was determined by a PL-MW2000 spectroradiometer (Perfect Light, China). The average power energy density of the irradiation light in this experiment was measured to be about 57.92, 64.19, 70.50, 77.01 and 81.24 mW/cm^2, respectively. The apparent QE was calculated using the ratio of the number of reacted electrons during hydrogen evolution to the number of incident photons by using the expression [36]:

$$\mathrm{QE} = \frac{2 \times \text{the number of evolved hydrogen molecules}}{\text{the number of incident photons}} \times 100\%.$$

3 Results and discussion

The powder XRD pattern of ZGP sample is shown in Fig. 1. It can be seen that all XRD peaks of ZGP are coincided with standard PDF No. 73-1235, and no impurities such as Ge, are detected, indicating that ZGP sample with good crystallization is obtained under the synthetic conditions of this paper. Figure 2 shows the SEM images of ZGP samples before and after the ultrasonic treatment. As can be seen from Fig. 2(a), prior to the ultrasonic treatment, most of ZGP samples are of irregular micron particles with large size. Figure 2(b) shows a representative larger particle with the particle size of ~20 μm in length, ~10 μm in width and ~3 μm in thickness. In addition, it is also found that there is several smaller size particles scattered on the surface of the large particles. However, the larger

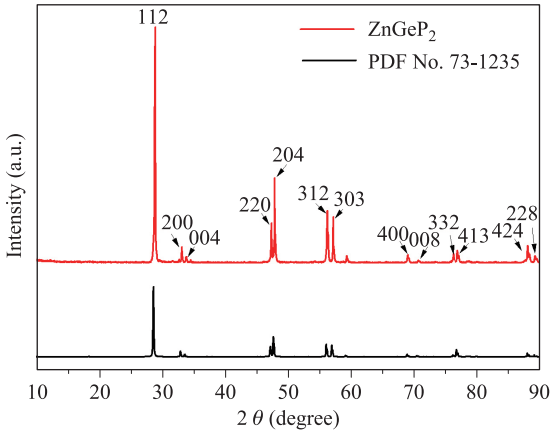

Fig. 1 The powder XRD pattern of ZGP sample.

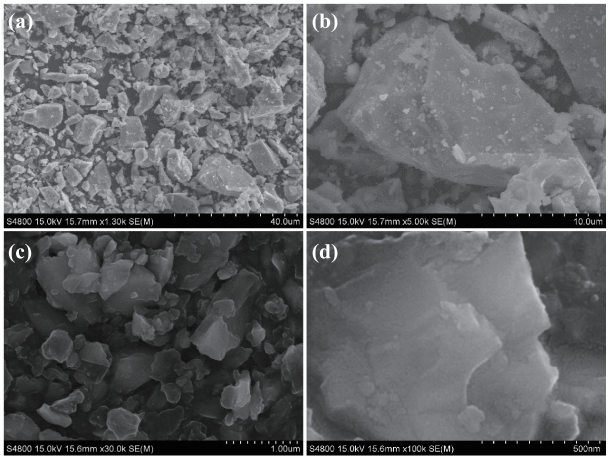

Fig. 2 The SEM images of ZGP **(a, b)** before and **(c, d)** after ultrasonic treatment.

ZGP particles were broken into smaller nanosheets with irregular shape by ultrasonic treatment, as shown in Figs. 2(c, d). Figure 3 shows the energy dispersive spectrometer (EDS) results and corresponding element content tables of ZGP samples before and after the ultrasonic treatment. It can be seen that the ZGP samples before and

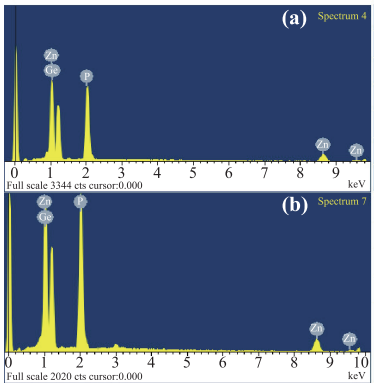

Element	weight %	Atonic %
P K	31.60	50.70
Zn L	32.72	24.88
Ge L	35.68	24.43
Totals	100.00	

Element	weight %	Atonic %
P K	31.54	50.07
Zn L	32.71	24.86
Ge L	35.75	25.07
Totals	100.00	

Fig. 3 The EDS and corresponding element content tables of ZGP **(a)** before and **(b)** after ultrasonic treatment.

after ultrasonic treatment both contain the only three elements of Zn, Ge and P, and the atomic content of Zn:Ge:P is approximately 1:1:2, which is close to the theoretical value. The above experimental results show that the ultrasonic treatment only changes the particle size of the samples, and have no effects on the element composition of the samples.

UV-Vis-NIR diffuses reflectance spectrum (DRS) and band gap energy (E_g) of ZGP sample are shown in Fig. 4. The results show that ZGP has a wide light absorption range covering both visible and near infrared regions, and its absorption band edge is about 1200 nm [Fig. 4(a)]. According to the DRS spectrum in Fig. 4(a), the band gap energy of ZGP sample can be calculated using the following formula: $\alpha h\nu = A(h\nu - E_g)^{\frac{n}{2}}$, where α, h, ν, E_g and A are the absorption coefficient, Plank constant, light frequency, band gap energy and a constant, respectively. And the value of n in above formula depends on the optical transition form of semiconductors ($n = 1$ is direct transition, $n = 4$ is indirect transition) [37]. It is reported that ZGP is a direct band semiconductor [38–41], so the E_g of ZGP can be determined from a plot of $(\alpha h\nu)^2$ versus energy ($h\nu$), as shown in Fig. 4(b), the value of E_g is 1.47 eV, which is larger than the earlier reported theoretical values of 1.1 eV [42–44]. The deviation between the theoret-

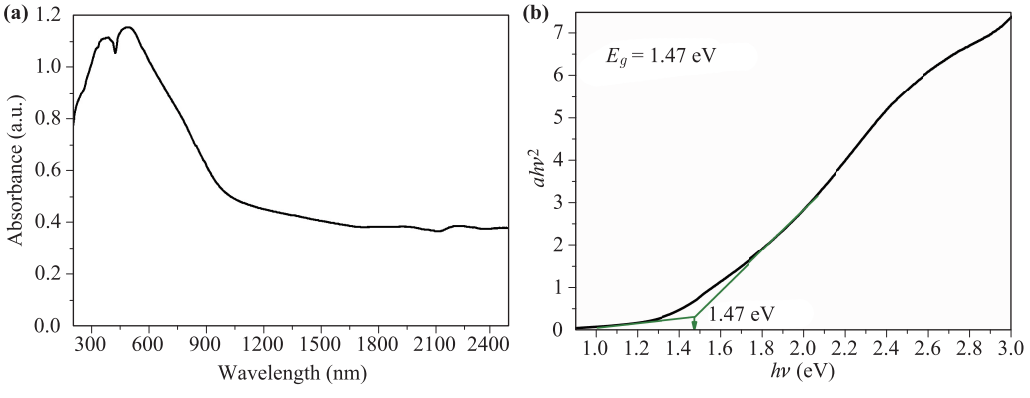

Fig. 4 **(a)** UV-Vis-NIR diffuses reflectance spectrum (DRS) and **(b)** band gap energy (E_g) of ZGP sample.

ical and experimental values is mainly due to the insufficient treatment of exchange correlation energy during calculating process by density functional theory [45, 46]. It is well known that the band structure of a semiconductor is closely related to its photocatalytic performance. Therefore, XPS valence band spectrum of the ZGP sample is also tested and the result is shown in Fig. 5. It can be seen that the valence band potential (E_{VB}) of ZGP is 0.548 eV, according to the formula: $E_{CB} = E_{VB} - E_g$ [47], the conduction band potential (E_{CB}) of ZGP can be calculated to be −0.922 eV. The E_{CB} of ZGP is far below the hydrogen evolution potential (0.00 eV), indicating that ZGP has sufficient power to reduce H^+ to H_2.

Figure 6 shows H_2 production of ZGP samples under visible light ($\lambda > 420$ nm) and near infrared light ($\lambda > 800$ nm) irradiation. According to Fig. 6(a), ZGP shows a weak photocatalytic H_2 production activity in methanol-water system. Even so, the amount of H_2 production stops increasing after 30 minutes of reaction, which is mainly because that ZGP is easily oxidized by photo-induced holes due to the existence of P^{3-}. When a certain amount of common stabilizer H_3PO_2 is added into this reaction system, the photocorrosion of ZGP is effectively alleviated, and the photocatalytic H_2 production activity and stability are obviously improved. In addition, we also find that the photocatalytic activity of ZGP treated by ultrasound is much better than that of ZGP before ultrasonic treatment, and the H_2 production rate is increased by about 2.5 times. In order to eliminate the effect of H_3PO_2 on the direct H_2 production of the system, we carried out a blank control experiment, namely, the H_2 production of the reaction system without any photocatalysts was tested. The results show that a bit amount of H_2 has also been detected, which is very small compared to the H_2 produced by ZGP photocatalytic reaction, and can be ignored. The H_2 production of ZGP samples under near infrared irradiation are also detected, as shown in Fig. 6(b). It can be seen that the ZGP sample also shows photocatalytic activity of H_2 production, and ZGP sample after ultrasonic treatment displays the best photocatalytic activity in the presence of common stabilizer H_3PO_2, which is in well agreement with the results of H_2 production under visible light irradiation.

The apparent quantum efficiency (AQE) of ZGP sample was measured to further evaluate its photocatalytic H_2 production performance, and a Xe arc lamp equipped with band-pass filters (420 nm, 450 nm, 520 nm, 600 nm or 850 nm) with a masked area of π cm^2 was used to provide light source. As shown in Fig. 7, the apparent quantum efficiencies for H_2 production of ZGP are 0.47%, 0.48%, 0.49%, 0.40%, and 0.18% at the wavelength of 420 nm, 450 nm, 520 nm, 600 nm, and 850 nm, respectively. In addition, the variation tendency of the AQE of ZGP sample is consistent with its light absorption. The photocatalytic hydrogen evolution of ZGP sample under the illumination of AM 1.5 G was also measured, as shown in Fig. 8. It can be seen that ZGP displays a certain photocatalytic activity in hydrogen production from water under simulated solar irradiation. All of the above experimental results show that ZGP is a promising photocatalyst for hydrogen production both in visible and near-infrared light irradiation.

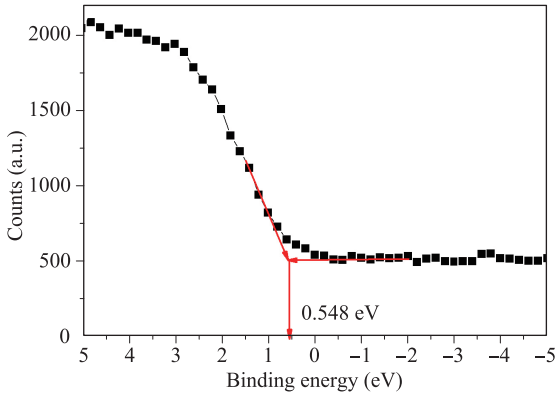

Fig. 5 The XPS valence band spectrum of ZGP sample.

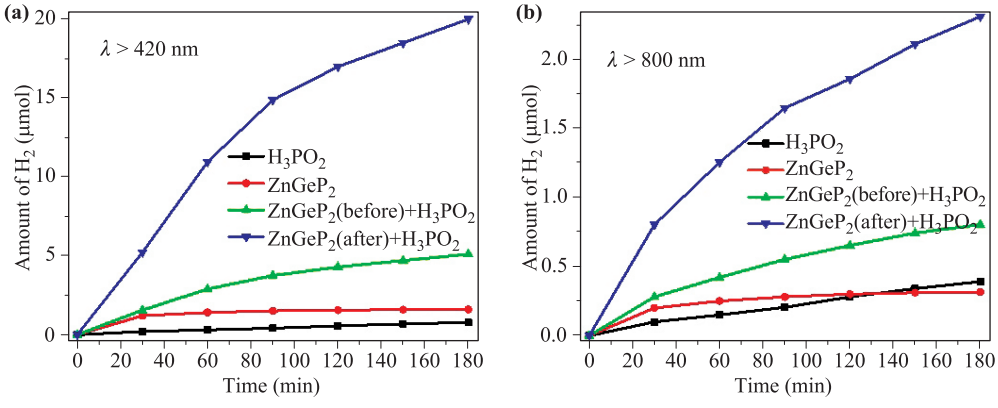

Fig. 6 Time courses of H_2 production under **(a)** visible light ($\lambda > 420$ nm) and **(b)** near infrared light ($\lambda > 800$ nm) irradiation.

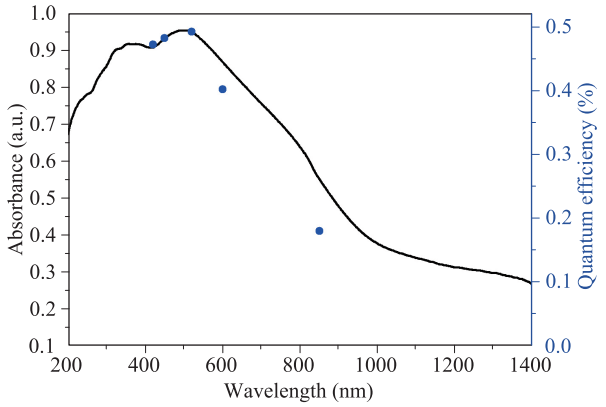

Fig. 7 UV-vis-NIR diffuses reflectance spectrum and quantum efficiencies of ZGP.

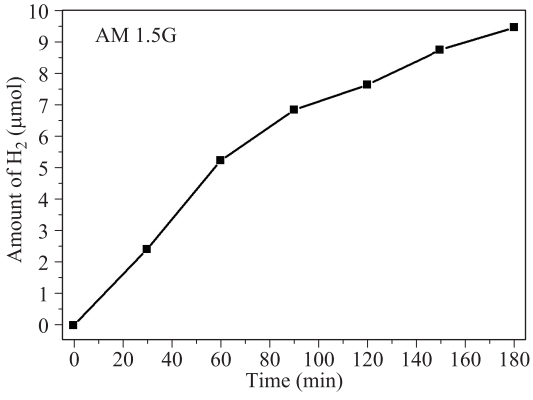

Fig. 8 Time courses of H_2 production of ZGP under the illumination of AM 1.5 G.

4 Conclusions

In summary, we prepared ZGP photocatalyst using single flat temperature zone (SFT) method in a vacuum quartz ampoule. The crystallization, morphology, light absorption and band structure of ZGP were also characterized, and the results display that ZGP meets the basic requirements of photocatalytic hydrogen production. The results of photocatalytic hydrogen evolution and apparent quantum efficiency show that ZGP is a potential photocatalyst for hydrogen production, both in visible and near-infrared light. Our work will provide a new insight for the design and exploration of near-infrared-activated photocatalysts for hydrogen production.

Acknowledgements This work was financially supported from the National Natural Science Foundation of China (Grant Nos. 21832005, 51602179, 51972195, 21972078, and U1832145), the Major Special Projects of Shandong Province (public welfare; 2019GGX103026). P. Wang acknowledges the support from the Recruitment Program of Global Experts, China, and B. Huang acknowledges the support from the Taishan Scholars Foundation of Shandong Province.

References

1. A. Fujishima and K. Honda, Electrochemical photolysis of water at a semiconductor electrode, *Nature* 238(5358), 37 (1972)
2. Q. T. Liu, D. Y. Liu, J. M. Li, and Y. B. Kuang, The impact of crystal defects towards oxide semiconductor photoanode for photoelectrochemical water splitting, *Front. Phys.* 14(5), 53403 (2019)
3. S. Q. Luo, J. F. Wang, B. Yang, and Y. B. Yuan, Recent advances in controlling the crystallization of two-dimensional perovskites for optoelectronic device, *Front. Phys.* 14(5), 53401 (2019)
4. Y. H. Lui, B. W. Zhang, and S. Hu, Rational design of photoelectrodes for photoelectrochemical water splitting and CO_2 reduction, *Front. Phys.* 14(5), 53402 (2019)
5. J. Mao, Y. Wang, Z. L. Zheng, and D. H. Deng, The rise of two-dimensional MoS_2 for catalysis, *Front. Phys.* 13(4), 138118 (2018)
6. J. Q. Pan, Z. J. Dong, B. B. Wang, Z. Y. Jiang, C. Zhao, J. J. Wang, C. S. Song, Y. Y. Zheng, and C. R. Li, The enhancement of photocatalytic hydrogen production via Ti^{3+} self-doping black TiO_2/g-C_3N_4 hollow core-shell nano-heterojunction, *Appl. Catal. B* 242, 92 (2019)
7. X. Li, X. S. Lv, Q. Q. Zhang, B. B. Huang, P. Wang, X. Y. Qin, X. Y. Zhang, and Y. Dai, Self-assembled supramolecular system PDINH on TiO_2 surface enhances hydrogen production, *J. Colloid Interface Sci.* 525, 136 (2018)
8. H. Q. Zhuang, Z. P. Cai, W. T. Xu, X. Y. Zhang, M. L. Huang, and X. X. Wang, Constructing 1D CdS nanorod composites with high photocatalytic hydrogen production by introducing the Ni-based cocatalysts, *Catal. Commun.* 120, 51 (2019)
9. L. L. Zhang, H. W. Zhang, B. Wang, X. Y. Huang, Y. Ye, R. Lei, W. H. Feng, and P. Liu, A facile method for regulating the charge transfer route of WO_3/CdS in high-efficiency hydrogen production, *Appl. Catal. B* 244, 529 (2019)
10. P. Zhou, Y. Y. Liu, Z. Y. Wang, P. Wang, X. Y. Qin, X. Y. Zhang, B. B. Huang, and Y. Dai, Efficient photocatalytic hydrogen generation from water over CdS nanoparticles confined within an alumina matrix, *ChemPhotoChem* 1(11), 518 (2017)
11. X. Z. Liang, P. Wang, M. M. Li, Q. Q. Zhang, Z. Y. Wang, Y. Dai, X. Y. Zhang, Y. Y. Liu, M. H. Whangbo, and B. B. Huang, Adsorption of gaseous ethylene via induced polarization on plasmonic photocatalyst Ag/AgCl/TiO_2 and subsequent photodegradation, *Appl. Catal. B* 220, 356 (2018)
12. K. C. Christoforidis, Z. Syrgiannis, V. La Parola, T. Montini, C. Petit, E. Stathatos, R. Godin, J. R. Durrant, M. Prato, and P. Fornasiero, Metal-free dual-phase full organic carbon nanotubes/g-C_3N_4 heteroarchitectures for photocatalytic hydrogen production, *Nano Energy* 50, 468 (2018)

13. J. Y. Chu, X. J. Han, Z. Yu, Y. C. Du, B. Song, and P. Xu, Highly efficient visible-light-driven photocatalytic hydrogen production on $CdS/Cu_7S_4/g\text{-}C_3N_4$ ternary heterostructures, *ACS Appl. Mater. Interfaces* 10(24), 20404 (2018)

14. Y. Q. Wu, P. Wang, X. L. Zhu, Q. Q. Zhang, Z. Y. Wang, Y. Y. Liu, G. Z. Zou, Y. Dai, M. H. Whangbo, and B. B. Huang, Composite of $CH_3NH_3PbI_3$ with reduced graphene oxide as a highly efficient and stable visible-light photocatalyst for hydrogen evolution in aqueous HI solution, *Adv. Mater.* 30(7), 1704342 (2018)

15. Z. H. Guan, Y. Q. Wu, P. Wang, Q. Q. Zhang, Z. Y. Wang, Z. K. Zheng, Y. Y. Liu, Y. Dai, M. H. Whangbo, and B. B. Huang, Perovskite photocatalyst $CsPbBr_{3-x}I_x$ with a bandgap funnel structure for H_2 evolution under visible light, *Appl. Catal. B* 245, 522 (2019)

16. T. Jing, Y. Dai, W. Wei, X. D. Ma, and B. B. Huang, Near-infrared photocatalytic activity induced by intrinsic defects in Bi_2MO_6 (M=W, Mo), *Phys. Chem. Chem. Phys.* 16(34), 18596 (2014)

17. J. Li, X. Y. Wu, W. F. Pan, G. K. Zhang, and H. Chen, Vacancy-rich monolayer BiO_{2-x} as a highly efficient UV, visible, and near-infrared responsive photocatalyst, *Angew. Chem. Int. Ed.* 57(2), 491 (2018)

18. J. Tian, Y. H. Sang, G. W. Yu, H. D. Jiang, X. N. Mu, and H. Liu, A Bi_2WO_6-based hybrid photocatalyst with broad spectrum photocatalytic properties under UV, visible, and near-infrared irradiation, *Adv. Mater.* 25(36), 5075 (2013)

19. Q. H. Liang, Z. Li, Z. H. Huang, F. Kang, and Q. H. Yang, Holey graphitic carbon nitride nanosheets with carbon vacancies for highly improved photocatalytic hydrogen production, *Adv. Funct. Mater.* 25(44), 6885 (2015)

20. X. Y. Kong, Y. Y. Choo, S. P. Chai, A. K. Soh, and A. R. Mohamed, Oxygen vacancy induced Bi_2WO_6 for the realization of photocatalytic CO_2 reduction over the full solar spectrum: From the UV to the NIR region, *Chem. Commun.* 52(99), 14242 (2016)

21. N. Manfredi, M. Monai, T. Montini, F. Peri, F. De Angelis, P. Fornasiero, and A. Abbotto, Dye-sensitized photocatalytic hydrogen generation: Efficiency enhancement by organic photosensitizer–coadsorbent intermolecular interaction, *ACS Energy Lett.* 3(1), 85 (2018)

22. Q. Y. Tian, W. J. Yao, W. Wu, J. Liu, Z. H. Wu, L. Liu, Z. G. Dai, and C. Z. Jiang, Efficient UV–Vis-NIR responsive upconversion and plasmonic-enhanced photocatalyst based on lanthanide-doped $NaYF_4/SnO_2/Ag$, *ACS Sustain. Chem. & Eng.* 5(11), 10889 (2017)

23. A. Kumar, K. L. Reddy, S. Kumar, A. Kumar, V. Sharma, and V. Krishnan, Rational design and development of lanthanide-doped $NaYF_4$ @CdS–Au–RGO as quaternary plasmonic photocatalysts for harnessing visible–near-infrared broadband spectrum, *ACS Appl. Mater. Interfaces* 10(18), 15565 (2018)

24. W. N. Wang, C. X. Huang, C. Y. Zhang, M. L. Zhao, J. Zhang, H. J. Chen, Z. B. Zha, T. T. Zhao, and H. S. Qian, Controlled synthesis of upconverting nanoparticles/$Zn_xCd_{1-x}S$ yolk-shell nanoparticles for efficient photocatalysis driven by NIR light, *Appl. Catal. B* 224, 854 (2018)

25. K. L. Reddy, S. Kumar, A. Kumar, and V. Krishnan, Wide spectrum photocatalytic activity in lanthanide-doped upconversion nanophosphors coated with porous TiO_2 and Ag-Cu bimetallic nanoparticles, *J. Hazard. Mater.* 367, 694 (2019)

26. Q. Y. Tian, W. J. Yao, W. Wu, and C. Z. Jiang, NIR light-activated upconversion semiconductor photocatalysts, *Nanoscale Horiz.* 4(1), 10 (2019)

27. M. S. Zhu, Y. Osakada, S. Kim, M. Fujitsuka, and T. Majima, Black phosphorus: A promising two dimensional visible and near-infrared-activated photocatalyst for hydrogen evolution, *Appl. Catal. B* 217, 285 (2017)

28. Z. J. Zhang and W. Z. Wang, Infrared-light-induced photocatalysis on $BiErWO_6$, *Dalton Trans.* 42(34), 12072 (2013)

29. G. C. Xi, S. X. Ouyang, P. Li, J. H. Ye, Q. Ma, N. Su, H. Bai, and C. Wang, Ultrathin $W_{18}O_{49}$ nanowires with diameters below 1 nm: Synthesis, near-infrared absorption, photoluminescence, and photochemical reduction of carbon dioxide, *Angew. Chem. Int. Ed.* 51(10), 2395 (2012)

30. L. Wei, X. S. Lv, Y. G. Yang, J. H. Xu, H. J. Yu, H. D. Zhang, X. P. Wang, B. Liu, C. Zhang, and J. X. Zhou, Theoretical investigation on the microscopic mechanism of lattice thermal conductivity of $ZnXP_2$ (X=Si, Ge, and Sn), *Inorg. Chem.* 58(7), 4320 (2019)

31. K. S. Rao, D. Ganesh, and A. K. Chaudhary, Generation of terahertz from $ZnGeP_2$ crystal and its application to record the time-resolved photoacoustic spectra of nitromethane, *Opt. Laser Technol.* 103, 126 (2018)

32. A. D. Martinez, A. N. Fioretti, E. S. Toberer, and A. C. Tamboli, Synthesis, structure, and optoelectronic properties of II–IV–V_2 materials, *J. Mater. Chem. A* 5(23), 11418 (2017)

33. M. Henriksson, M. Tiihonen, V. Pasiskevicius, and F. Laurell, $ZnGeP_2$ parametric oscillator pumped by a linewidth-narrowed parametric 2 μm source, *Opt. Lett.* 31(12), 1878 (2006)

34. M. Gebhardt, C. Gaida, P. Kadwani, A. Sincore, N. Gehlich, C. Jeon, L. Shah, and M. Richardson, High peak-power mid-infrared $ZnGeP_2$ optical parametric oscillator pumped by a Tm:fiber master oscillator power amplifier system, *Opt. Lett.* 39(5), 1212 (2014)

35. M. W. Haakestad, H. Fonnum, and E. Lippert, Mid-infrared source with 0.2 J pulse energy based on nonlinear conversion of Q-switched pulses in $ZnGeP_2$, *Opt. Express* 22(7), 8556 (2014)

36. Z. X. Qin, F. Xue, Y. B. Chen, S. H. Shen, and L. J. Guo, Spatial charge separation of one-dimensional Ni_2P-$Cd_{0.9}Zn_{0.1}S/g\text{-}C_3N_4$ heterostructure for high-quantum-yield photocatalytic hydrogen production, *Appl. Catal. B* 217, 551 (2017)

37. J. Zeng, H. Wang, Y. C. Zhang, M. K. Zhu, and H. Yan, Hydrothermal synthesis and photocatalytic properties of pyrochlore $La_2Sn_2O_7$ nanocubes, *J. Phys. Chem. C* 111(32), 11879 (2007)
38. S. R. Zhang, D. P. Zeng, H. J. Hou, and Y. Yu, First-principles prediction on elastic anisotropic, optical, lattice dynamical properties of $ZnGeP_2$, *Indian J. Phys.* (2019), doi:10.1007/s12648-019-01575-8
39. F. Herman and S. Skillman, Atomic Structure Calculations, Prentice Hall, Englewood Cliffs, New Jersey, 1966
40. R. R. Reddy, K. R. Gopal, K. Narasimhulu, L. S. S. Reddy, K. R. Kumar, G. Balakrishnaiah, and M. R. Kumar, Interrelationship between structural, optical, electronic and elastic properties of materials, *J. Alloys Compd.* 473(1-2), 28 (2009)
41. S. K. Tripathy and V. Kumar, Electronic, elastic and optical properties of $ZnGeP_2$ semiconductor under hydrostatic pressures, *Mater. Sci. Eng. B* 182, 52 (2014)
42. S. N. Rashkeev, S. Limpijumnong, and W. R. L. Lambrecht, Second-harmonic generation and birefringence of some ternary pnictide semiconductors, *Phys. Rev. B* 59(4), 2737 (1999)
43. F. Chiker, B. Abbar, S. Bresson, B. Khelifa, C. Mathieu, and A. Tadjer, The reflectivity spectra of $ZnXP_2$ (X=Si, Ge, and Sn) compounds, *J. Solid State Chem.* 177(11), 3859 (2004)
44. J. E. Jaffe and A. Zunger, Electronic structure of the ternary pnictide semiconductors $ZnSiP_2$, $ZnGeP_2$, $ZnSnP_2$, $ZnSiAs_2$, and $MgSiP_2$, *Phys. Rev. B* 30(2), 741 (1984)
45. G. Kalpana, B. Palanivel, R. M. Thomas, and M. Rajagopalan, Electronic and structural properties of MgS and MgSe, *Physica B* 222(1-3), 223 (1996)
46. R. W. Godby, M. Schlüter, and L. J. Sham, Self-energy operators and exchange-correlation potentials in semiconductors, *Phys. Rev. B* 37(17), 10159 (1988)
47. X. Zhang, L. Z. Zhang, T. F. Xie, and D. J. Wang, Low-temperature synthesis and high visible-light-induced photocatalytic activity of $BiOI/TiO_2$ heterostructures, *J. Phys. Chem. C* 113(17), 7371 (2009)